CONSERVAR PATRIMÓNIO

ARTICLE / ARTIGO

Analytical investigation and electrochemical conservation treatment for archaeological copper alloy artifacts from Jordan

Investigação analítica e tratamento eletroquímico de conservação em bens arqueológicos de liga de cobre da Jordânia

AHMAD N. ABU-BAKER

Department of Conservation and Management of Cultural Resources, Faculty of Archaeology and Anthropology, Yarmouk University, P.O. Box 566, Irbid 21163, Jordan

ahmad.abubaker@yu.edu.jo

Abstract

This study presents an analytical investigation and electrochemical conservation treatment for a group of four copper alloy artifacts excavated from the archaeological cemetery that was located on the site of the Queen Alia International Airport, Jordan. The chemical analyses of internal alloys showed that a bracelet and a spatula were made of a quaternary copper–zinc–tin–lead alloy, a bracelet was made of a copper–silver–zinc alloy, and a spatula was made of a copper–tin, a bronze alloy. The corrosion products analyses indicated the presence oxides, carbonates and chlorides of copper, in addition to silver chlorides for the copper–silver–zinc alloy bracelet. The metallographic examination showed various degrees of working and heat treatment in the manufacturing process of the artifacts. The potentiostatic reduction technique was effective in reducing the corrosion products on the artifacts, which were finally coated with Paraloid B–72 to prevent corrosion reoccurrence.

KEYWORDS

Copper alloy
Silver alloy
Archaeological artifacts
Corrosion
Examination
Conservation treatment

Resumo

Este estudo apresenta uma investigação analítica e o tratamento eletroquímico de conservação usado num grupo de quatro artefactos em liga de cobre, escavados no cemitério arqueológico localizado no aeroporto internacional Rainha Alia, Jordânia. As análises químicas das ligas internas mostraram que uma pulseira e uma espátula foram feitas com uma liga quaternária de cobre, zinco, estanho e chumbo, outra pulseira foi feita com uma liga de cobre, prata e zinco, e uma segunda espátula com uma liga de cobre e estanho (bronze). As análises dos produtos de corrosão indicaram a presença de óxidos, carbonatos e cloretos de cobre, além de cloretos de prata na pulseira em liga de cobre, prata e zinco. O exame metalográfico mostrou vários graus de manufatura e de tratamento térmico no processo de fabrico dos artefactos. A técnica de redução potenciostática foi eficaz na redução dos produtos de corrosão nos artefactos, que no final foram revestidos com Paraloide B72 para evitar a recorrência da corrosão.

PALAVRAS-CHAVE

Liga de cobre
Liga de prata
Bens arqueológicos
Corrosão
Exame analítico
Tratamento de conservação

Introduction

Copper alloy artifacts form an important part of our cultural heritage. Analytical studies are essential to understand their chemical, physical, and mechanical characteristics, and the use of safe and cost–effective conservation techniques is vital to protect them in our heritage collections. The corrosion of these artifacts is affected by several factors, such as the nature of their archaeological context, the presence and amounts of alloying elements, and their manufacturing techniques. In addition, the environmental conditions of the storage or exhibition area after excavation contribute to the activation or acceleration of the corrosion processes. Therefore, the analytical investigation of these artifacts provides essential information on their composition, microstructure, and corrosion processes, it clarifies their particular characteristics and allows elaborate determination of their preservation state and conservation needs [1–4].

The stabilization of corroded archaeological copper alloy artifacts is an essential primary treatment in the practical applications of the conservation profession, particularly, the stabilization of the active corrosion process commonly known as bronze disease. This corrosion process results from the oxidative hydrolysis of cuprous chlorides (CuCl) to form basic cupric chlorides ($Cu_2(OH)_3Cl$), which also recycles the chlorides released by hydrolysis, which in turn attack the uncorroded metal in a new cycle of corrosion in moist air. In practice, the adverse effect of the chloride–based corrosion could be reversed by removing the cuprous chlorides, sealing them from the atmosphere to stop the active corrosion, or converting them to the stable cuprous oxide [5–7]. The removal of cuprous chloride by the tedious mechanical cleaning or the uncontrollable corrosion stripping agents would cause several problems, such as the possible breakage or disintegration of the object, the overcleaning that leads to a shiny bare metal surface that distorts the aesthetic and historic values of the artifact, and the possible presence of residual chlorides or chemical cleaning agents in the crevices, which causes corrosion reoccurrence [8–10]. The common approach to seal the cuprous chloride from the atmosphere is using corrosion inhibitors. This treatment has the benefit of stabilizing the corrosion products on the surface, which causes less changes on the aesthetic and historic values of the artifact. However, a very limited number of corrosion inhibitors are used in practice, which is attributed to limitations in the effectiveness, the potential harmful or toxic nature of these chemicals, and the need for more testing results for the recently investigated compounds as corrosion inhibitors [11–21]. The immersion of the corroded artifact in a diluted solution of sodium sesquicarbonate has been a common stabilization treatment that removes the chlorides from the artifact and forms a stable cuprous oxide on its surface. The treatment could need months or years to be effective in removing a significant amount of chloride ions from the artifact, it may also cause the formation of blue–green malachite or black cupric oxide on the artifact's surface, which will affect the color of the patina [5–9]. The electrolytic potentiostatic reduction with weak polarization in a sodium sesquicarbonate solution was suggested for a faster extraction of the chloride ions while preserving the stable corrosion products such as cuprite and the copper hydroxycarbonates [22–24]. The treatment causes reduction in size and change in the appearance of the external corroded surface of the artifact. It was found that most of the chloride–based corrosion products become detached and dissolve in the electrolyte, and the cuprite forms only in the original interface region. Moreover, patches of the corrosion products of the alloying elements of copper, or their reduction products, would affect the appearance of the artifact after the treatment, and they cannot be mechanically removed without affecting the intentionally left stable copper corrosion products [25–26]. The electrolytic potentiostatic reduction on a potential sufficient for a complete reduction of all identified corrosion products of copper or its alloying metals while avoiding hydrogen evolution is another alternative. The treatment cleanses the artifact from the chloride ions, preserves surface details that characterize the artifact and its cultural values, and produces reduced metallic forms that clarify the original metallic identity of the artifact's surface without

obliterating its antique appearance. The treatment is very beneficial for copper alloy artifacts, particularly copper–silver alloys with high silver surface content as the galvanic corrosion products of copper will hide the original silvery surface. Based on the condition of the artifact after the treatment, the reduced powdery metal(s) can either be cleaned or fixed on the surface by an adhesive [27–30].

This study aimed to analytically investigate and electrochemically treat a group of four copper alloy artifacts excavated from the archaeological cemetery that was located on the site of the Queen Alia International Airport, Jordan. The analytical investigation helped to identify corrosion and microstructural properties of the artifacts, while the electrochemical treatment followed by the application of a protective coating were conducted to ensure their long-term stability in the uncontrolled environment of their storage area.

Materials and methods

The artifacts investigated in this study belong to the collections of the Museum of Jordanian Heritage at Yarmouk University, Irbid, Jordan. They were originally discovered in a rescue excavation that was conducted at a latesecond– early third CE century cemetery site, which was discovered during the construction works of the Queen Alia International Airport, about 25 km south of Amman, back in 1978. The cemetery occupied an area of about 65 m^2, it was part of a broader complex of remains that included a seasonal habitation site on the hills located to the east of the cemetery. The pottery on the hills indicated that the site was used during the Roman period. The cemetery was discovered during the leveling of the maintenance hangar area of the new airport, it consisted of 173 graves that contained skeletons, cremation lead ossuary, items of clothing and jewelry, seals, amulets, cosmetic equipment, toilet articles, tools, figurines, coins and shells [31]. The group of artifacts under investigation in this study includes two copper alloy bracelets and two copper alloy spatulas (Figure 1), they are relatively corroded, and no previous analyses or conservation treatments have been conducted on them since their acquisition and placement in the storage area of the museum.

The mineralogical composition of corrosion products on the artifacts was examined by X–ray diffraction (XRD) and/or scanning electron microscopy/energy dispersive X–ray spectroscopy (SEM/EDX). For the twisted–strands bracelet, a sample collected from the pale green powdery corrosion spots was analyzed using a Shimadzu LabX, XRD–6000 X-ray diffractometer to determine its mineralogical composition. The X–ray was generated from an anticathode Cu tube with a wavelength CuK_{α}= 1.5418 Å. The analysis range was 10°–80° 2θ and the scan speed was 2° per minute. The powdery corrosion products on the other three artifacts were not sufficient for XRD sampling. The elemental composition of the corrosion layers and original alloys of all artifacts were examined by SEM/EDX. Small cross–sections were taken from a strand of the twisted–strands bracelet, the spiral around the end of the snake–shaped bracelet, and the edges of the two spatulas using a fine jeweler's saw. The cross–sections were embedded in an Araldite 2020 epoxy resin. After 24 hours curing period, they were ground on silicon carbide papers down to 3000 grit, then gradually polished using 9–0.25 μm alumina suspensions and diamond pastes. The samples were ultrasonically cleaned in ethanol and finally dried. The SEM/EDX analysis was executed using a FEI–Quanta 200 analyzer.

The embedded cross–sections were also examined using an Optika IM-3MET inverted metallurgical microscope to investigate their corrosion profile. They were then etched with alcoholic ferric chloride to investigate their microstructures using cross-polarized light microscopy (PLM) to determine the manufacturing technique [32]. PLM photomicrographs were captured using an Optika C–P8 digital camera attachment.

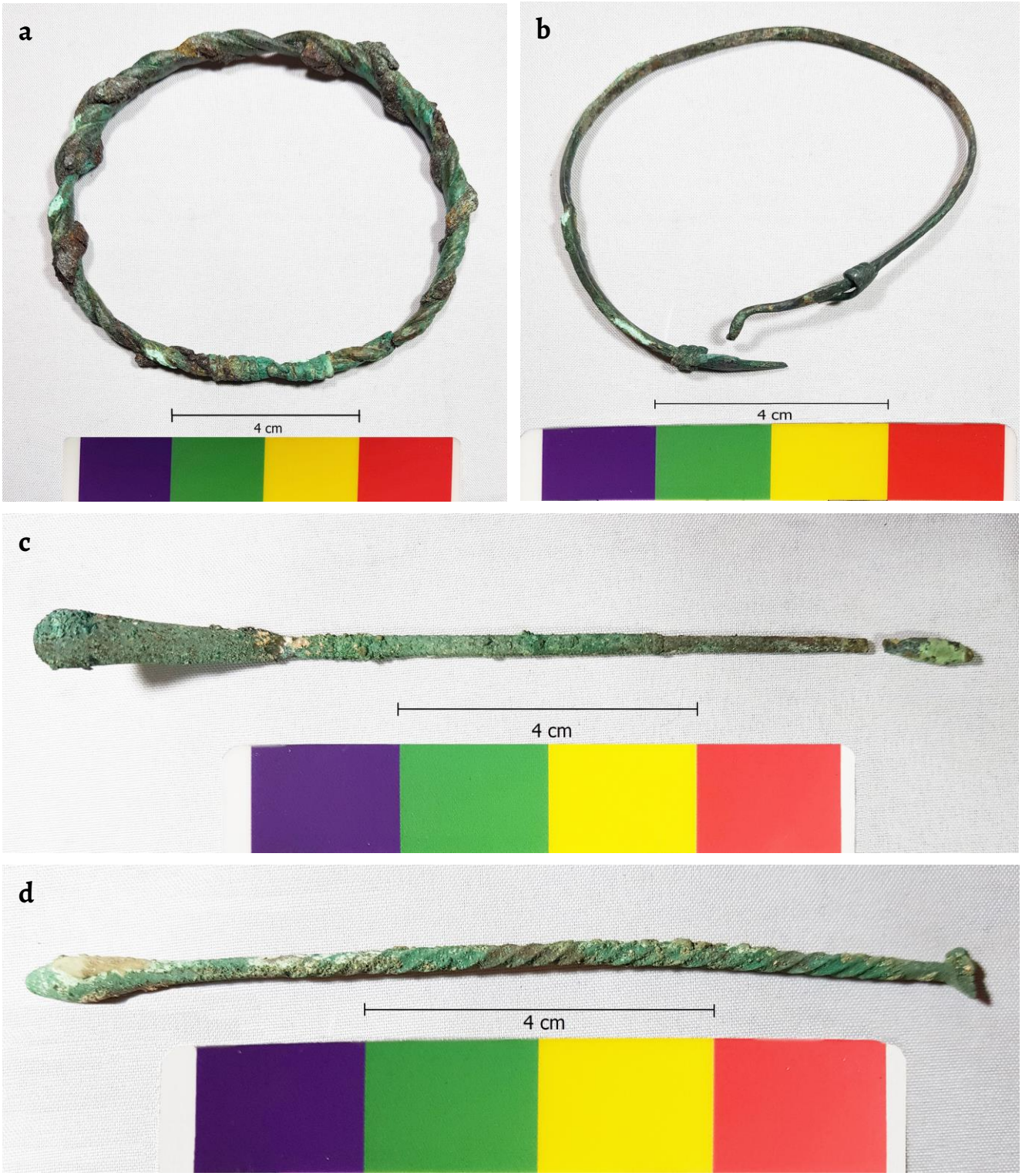

Figure 1. Before the stabilization treatment: *a)* twisted–strands bracelet; *b)* snake–shaped bracelet; *c)* flat–spoon spatula; *d)* twisted–handle spatula with a missing spoon.

The microhardness of the internal uncorroded alloy of the cross–sections was measured using a digital micro–Vickers hardness tester (HVD–1000 M). A diamond indenter was used for the microhardness testing and the measurements were obtained using a 4.904 N load with a 15 s dwell time. The microhardness measurements were calculated from the average values of six points measured for each sample [20].

Determining the potentiostatic reduction parameters of the corrosion products on the artifacts was carried out by potentiodynamic polarization scans in the cathodic direction from

the corrosion potential (E_{corr}) to −1.8 V vs the mercury/ mercurous sulfate (Hg/Hg_2SO_4) reference electrode filled with saturated potassium sulfate (10 % w/w) (Gamry Instruments) with a scanning rate of 1.0 mV/s. The potential of the reference electrode is 0.615 V vs the normal hydrogen electrode (NHE). A three−electrode electrochemical cell connected to a potentiostat (Vertex, Ivium Technologies, The Netherlands) was prepared. For each artifact, one liter of a 1 % w/v sodium sesquicarbonate dihydrate ($Na_3H(CO_3)_2{\cdot}2H_2O$) solution was used as the electrolyte. Each artifact was completely submerged in the electrolyte and held by a copper wire wrapped around it and connected to the alligator clip of the working electrode's wire outside the electrolyte. A stainless−steel mesh (T-316) with a surface area equaling or bigger than the surface area of the artifact was used as the counter electrode in the electrochemical cell. The immersion of the whole object in the electrolyte allowed to overcome the variability of the surface microtopography and underlying microstructures. It should be noted that referring to standard reduction potentials for the copper and silver minerals to interpret the reduction peaks appearing in the cathodic polarization curves is indicative but not conclusive, which is attributed to the presence of mixtures of corrosion products on the artifacts, which could overlap in their reduction peaks, however the XRD and SEM/EDX analyses results and the available literature data aided in the interpretation of the appearing peaks. Before the electrochemical treatments, the artifacts were degreased in acetone to ensure complete wetting of the surfaces.

Based on the cathodic polarization scan results, the potentiostatic reduction process was carried out at −1.4 V for all artifacts, which was sufficient to assure a complete reduction of all identified corrosion products while avoiding hydrogen evolution that might obliterate the surfaces during the treatment. The reduction process was monitored by chronoamperometry (CA) to determine the endpoint of the treatment, which is achieved by having a low and stable current value indicating the completion of the reduction process [24, 28, 30]. Following the potentiostatic reduction process, the artifacts were rinsed with deionized water with gentle brushing to clean the reduction residues and improve their appearance. To restore a unified silvery appearance of the snake−shaped bracelet after the treatment, the reduced copper spots on the surface were removed by wiping using cotton swabs moistened with a diluted solution of silver nitrate ($AgNO_3$).

Finally, the artifacts were cleaned with deionized water followed by dehydration in acetone. Since the artifacts' storage area is not environmentally controlled, they were coated with Paraloid B72 to protect them against environmental agents of deterioration that may cause corrosion such as high relative humidity and pollutant gases, and the edge of the flat−spoon spatula was fixed to its handle using a 20 % Paraloid B72 adhesive.

Results and discussion

Examination of the artifacts' corrosion products by XRD and/or SEM/EDX

The XRD characterization of the corrosion sample taken from the twisted−strands bracelet shows the presence of atacamite/paratacamite (α and γ−$Cu_2(OH)_3Cl$), cuprite (Cu_2O), and malachite ($CuCO_3.Cu(OH)_2$) as the main corrosion products (Figure 2). Cuprite is the first forming corrosion product on copper alloy surfaces in the presence of oxygen and moisture. The presence of malachite indicates a high carbonate content in the burial soil of the artifacts, it is anticipated to form in carbonate−rich soils with pH >7.5 [20, 33], while the presence of chloride−based corrosion products suggests that dissolved chlorides ions in the surrounding soil caused the formation of powdery atacamite/paratacamite minerals in the active corrosion process commonly known as bronze disease. The loss of parts of these powdery corrosion products formed corrosion pits in the surface of the artifact. As this corrosion reaction is active in the presence of oxygen and humidity in the surrounding environment, it can continue until it completely destroys the artifact [20, 34−37]. Similar powdery green corrosion spots are

appearing on the other three artifacts, which suggests a similar corrosion mechanism, however the corrosion products on those artifacts were not sufficient for XRD sampling. The presence of quartz (SiO_2) and calcite ($CaCO_3$) in the XRD analysis result is attributed to contamination with soil minerals from the burial environment.

For the SEM/EDX analysis, the SEM images of the cross–section taken from the twisted–strands bracelet show an external corrosion layer followed by internal corrosion pits above the uncorroded alloy (Table 1). The EDX analysis of the internal alloy shows that it is made of a quaternary copper–zinc–tin–lead alloy (Table 2). The small white islets present in the SEM image are the alloy α–phase insoluble lead (Pb) globules. Lead is added to reduce the melting point and increase the fluidity of the molten alloy, which results in better quality casts, therefore facilitating its casting process, while the small amounts of tin and zinc are soluble in the α–phase and increase the strength and hardness of the alloy [38–39]. Investigating the external corroded parts of the cross–section shows that the principal corrosion mechanism is intergranular corrosion. The presence of lead globules at the grain boundaries of the alloys has formed weakness areas where the intergranular corrosion proceeds [32]. The EDX analysis of the external corrosion layer shows the presence of carbon and oxygen, which possibly indicates the presence of oxide and carbonate corrosion products such as cuprite (Cu_2O) and malachite ($Cu_2CO_3(OH)_2$) (Table 2). The EDX analysis of the next corrosion area appearing as deep corrosion pits between the crystals shows a tin and zinc rich zone with the presence of chlorine (Table 2), which suggests a decuprification process causing copper depletion from the alloy during the active chloride–based corrosion process. The chloride containing burial environment in the archaeological site would have promoted the mobilization of the soluble $CuCl_2^-$ complex outside the alloy, which then underwent oxidative hydrolysis to the powdery basic cupric chlorides ($Cu_2(OH)_3Cl$) detected in the XRD analysis [34–37].

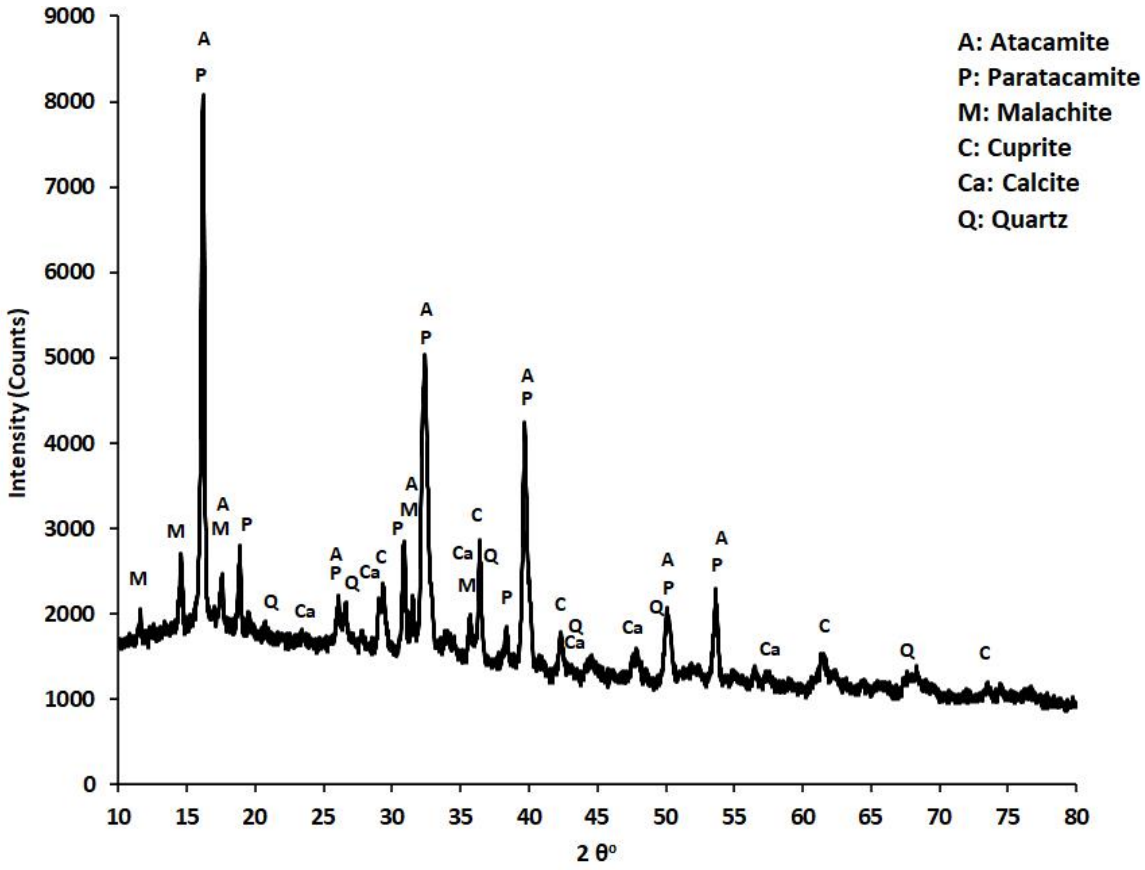

Figure 2. XRD analysis of the twisted–strands bracelet corrosion products.

The SEM images of the cross–section taken from the snake–shaped bracelet shows two alloy zones covered with an outer corrosion layer. The internal alloy zone is less porous than the external zone (Table 1). The EDX analysis of the inner zone marked (a) shows the presence of copper (70.9 wt. %), silver (20 wt. %), zinc (8.7 wt. %), and a small amount of tin (0.4 wt. %) (Table 2). The dark gray structure is the α–copper rich dendrites, while the light gray infill is the silver rich α+β eutectic structure, which were confirmed by EDX spot analyses. For the external porous alloy zone marked (b), the wt. % of copper decreases to 34.1 %, and the silver wt.% increases to 54.6 % with the presence of 10.6 % Cl and 0.7 % O (Table 2). This suggests that the bracelet is made of a silver–copper–zinc alloy that had its surface enriched with silver by the depletion silvering method; a technique that includes alternating hammering, annealing, and pickling off the surface copper and zinc oxides formed to obtain a silvery outer surface, i.e. the near surface zone below the surface corrosion products is rich in silver, which in the uncorroded state was giving the bracelet the appearance of pure silver, although the average silver content of the original copper–silver alloy is about 20 % [40–41]. The presence of chlorine in the EDX analysis for the external alloy zone marked (b) in Table 1 and the presence of powdery pale green corrosion spots at the surface of the bracelet suggest a galvanic corrosion mechanism which led to an acceleration in the corrosion of the anodic metal, copper, at the residual α–copper rich dendrites of the external copper depleted zone, while protecting the cathodic silver rich eutectic microconstituent. The selective dissolution of copper into the surrounding environment was followed by a formation of copper enriched layer with the redeposition of corroded copper onto the surface in the form of corrosion products. The powdery pale green corrosion products are possibly the basic cupric chlorides that formed by the oxidative hydrolysis of cuprous chloride in the active corrosion process commonly known as bronze disease. Although silver is the cathodic metal in galvanic Ag–Cu couple, it can also suffer corrosion because of local action cells and forms insoluble AgCl patches in the external Ag rich zone [30, 42–43]. The SEM/EDX analysis of the corrosion products extended beyond the original surface of the cross–section (Table 1: 2.2 area (a), Table 2) shows the presence of Cu (74.5 %), C (5.5 %), and O (19 %) which possibly suggests the presence of copper oxides and basic cupric carbonates such as malachite that appears as a blue–green corrosion layer obscuring the original silvery appearance of the bracelet.

The SEM/EDX analysis of the internal sound alloy in the cross–section taken from the flat–spoon spatula shows that it is made of a quaternary copper–zinc–tin–lead alloy (Table 1 and Table 2). Tin is present in a small amount (0.8 %), therefore it could be considered a leaded brass artifact in terms of historic metallurgy. The small amount of tin could have come from the smelting of tin containing copper ore, or because of recycling scrap bronze in the manufacture of the object [44–45]. The SEM image of the internal alloy shows several white globules, which were identified as lead by an EDX spot analysis. The SEM/EDX analysis at the area marked (a) in the corrosion blister at the edge of the cross–section in Table 1 shows the presence of copper, oxygen, and chlorine (Table 2), which possibly indicates a basic cupric chlorides corrosion blister resulting from the active chloride–based corrosion of copper. The SEM/EDX analysis of the internal corroded area marked (b) in Table 1 shows that it is chloride–based and is rich in zinc and lead. Oxygen and carbon are also detected which strongly indicates oxide and carbonate corrosion products (Table 2). This suggests that the corrosive attack is also causing the leaching of zinc towards the external layer [20, 46]. The high concentration of lead in the outer layer of the alloy indicates the artifact was initially cast in a mold where it was allowed to slowly cool, and due to gravity segregation pooled down to the bottom of the mold and solidified in the external part of the alloy [47].

Table 1. SEM images of the internal alloys and corroded edges of the artifacts.

Artifact	Internal alloy	Corroded edge
Twisted–strands bracelet	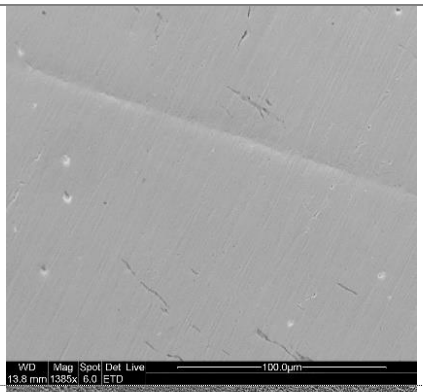	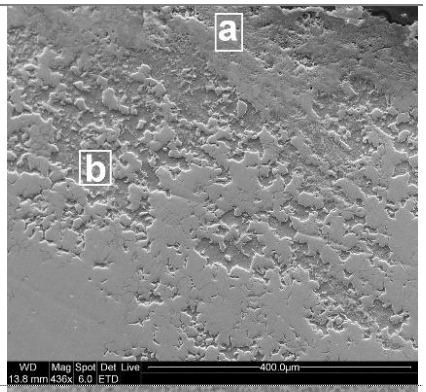
Snake–shaped bracelet	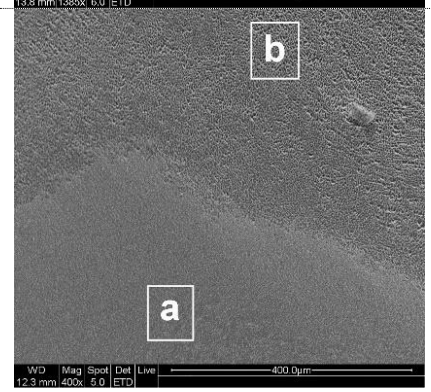	
3.Flat–spoon spatula	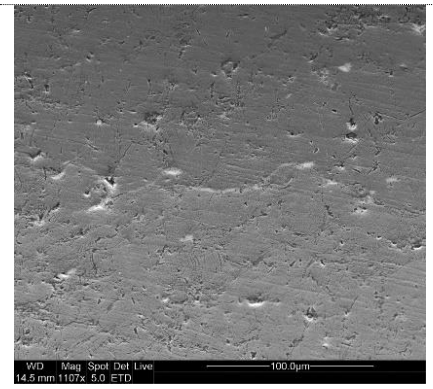	
Twisted–handle spatula	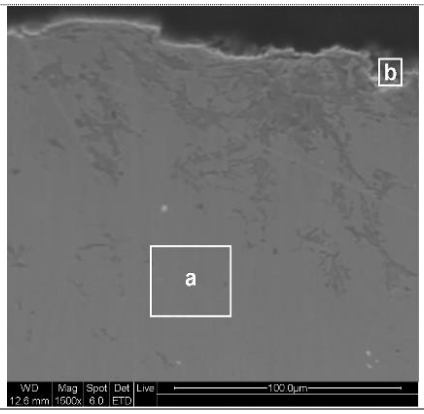	

Table 2. EDX analysis results (wt. %) for the alloys and corroded edges of the artifacts.

Artifact	Analyzed area	Elements									
		Cu	Sn	Zn	Pb	Ag	O	C	Cl	Mg	S
Twisted–strands bracelet	Internal alloy (full frame)	89.3	2.1	1.1	7.4						
	Corroded edge (area (a))	58.3	0.7	5.2	25.9		8.1	1.8			
	Corroded edge (area (b))	76.6	6.3	10.1			2.9	1.4	2.7		
Snake–shaped bracelet	Internal alloy zone (area (a))	70.9	0.4	8.7		20.0					
	External alloy zone (area (b))	34.1				54.6	0.7		10.6		
	Corroded edge area (a)	74.5					19.0	5.5		0.9	
Flat–spoon spatula	Internal alloy (full frame)	72.7	0.8	14.1	12.4						
	Corroded edge (area (a))	82.2					1.7		16.1		
	Corroded edge (area (b))	17.6	2.0	41.1	29.4		6.0	1.1	2.8		
Twisted–handle spatula	Internal alloy (area (a))	89.5	9.2								1.3
	Corroded edge (area (b))	90.2	3.5				1.8	3.4	1.1		

The SEM/EDX analysis of the internal sound alloy in the cross–section taken from the twisted handle spatula shows that it is made of a tin–bronze alloy (Table 1 and Table 2). The SEM image shows the presence of darker areas in the alloy, which are associated with the presence of the tin–rich α+δ eutectoid. The presence of S in the EDX analysis is associated with the presence of some unrefined copper sulfide ore inclusions. The EDX analysis of the external corroded area marked (b) shows the presence of carbon, oxygen, and chlorine which may indicate the presence of copper oxides, basic carbonates, and basic chlorides as the corrosion products of this artifact (Table 2). This suggests a decuprification of the copper rich α–phase, which is consistent with an oxygenated burial microenvironment. It seems that the tin (IV) oxide remained as a primary thin corrosion layer underneath the secondary copper corrosion layer. In the chloride–based corrosion of bronze, when the unstable $SnCl_3^-$ ions reach the external environment they undergo oxidative hydrolysis to produce the solid SnO_2 which has higher thermodynamic stability, while the more soluble copper minerals migrate to the margin and form external corrosion products [48–49].

Examination using the polarizing microscope

For the twisted–strands bracelet, the PLM image of the unetched cross–section shows a number of corrosion layers and features at the external edge; an external green layer that includes the malachite ($Cu_2CO_3(OH)_2$) and atacamite/paratacamite (α and γ–$Cu_2(OH)_3Cl$) corrosion products, a red–brown cuprite (Cu_2O) patina followed by internal yellow–orange nantokite (CuCl) located at the interface between exterior corrosion layers and internal alloy and along the grain boundaries (Figure 3a) [50–51], which conforms with the XRD and SEM/EDX analysis results. The dark gray phase is rich in zinc and tin as clarified in the SEM/EDX examination, and the white spots are the oxidized lead globules. The image shows a directional pattern for the in Zn–Sn rich phase, lead globules, and the intergranular corrosion cracks, which complies with the twisted nature of the bracelet strands and indicates that the working stress was not completely released in the annealing process.

The PLM examination of the etched internal alloy of the twisted–strands bracelet shows recrystallized equiaxed α–grains with the presence of annealing twins, which resulted from the working and annealing of the artifact in the manufacturing process (Figure 3b). Several lead globules are also appearing as white spots as a result of the etching process. The small grains indicate several cycles of working and annealing, which was finalized with an annealing stage as indicated by the presence of straight annealing twins. The working process caused elongation in the lead globules and coring in the copper rich α–phase was not completely removed by the annealing process of this twisted bracelet [47].

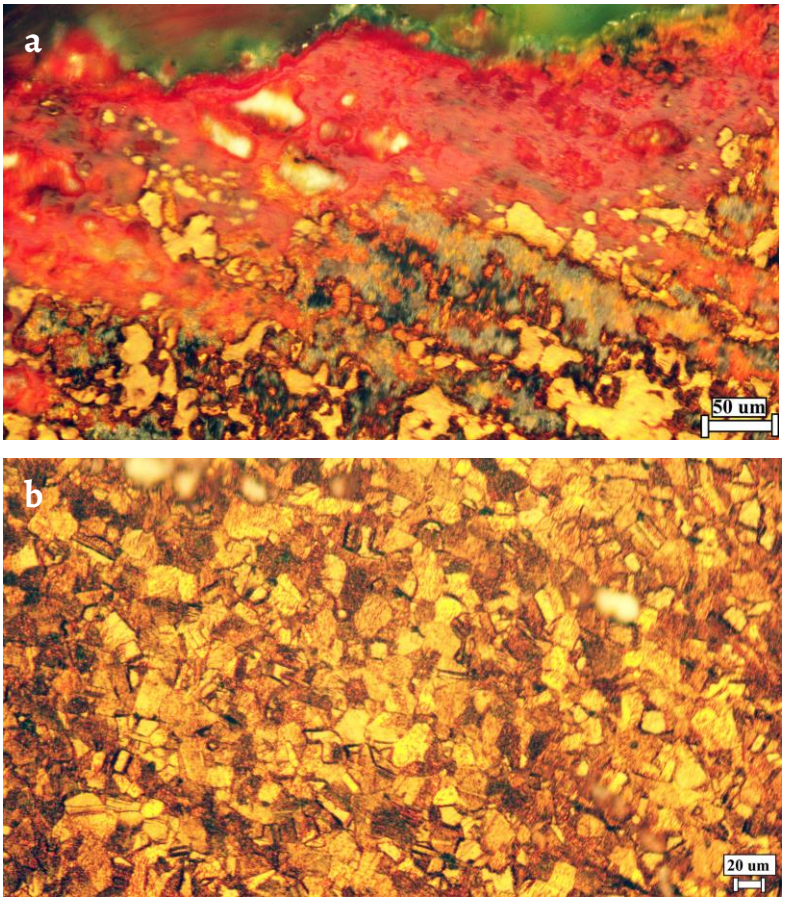

Figure 3. PLM images of twisted–strands bracelet: *a)* the unetched corroded edge; *b)* etched internal alloy.

For the snake–shaped bracelet, the PLM images show an external copper based green corrosion products and internal binary microstructure, typical of copper–silver alloys below the eutectic composition, which contain α–Cu rich dendrites with an infill of a silver rich α+β eutectic. The copper–silver–zinc alloy was most likely surface–enriched with silver by pickling, resulting in copper and zinc depletion at the external area (Figure 4). The depletion silvering was confirmed by the SEM/EDX analysis results. The dendritic segregation of this alloy persists and does not disappear despite the working and annealing process, which causes distortion or flattening in the dendrites along the fabrication direction [32, 52–53].

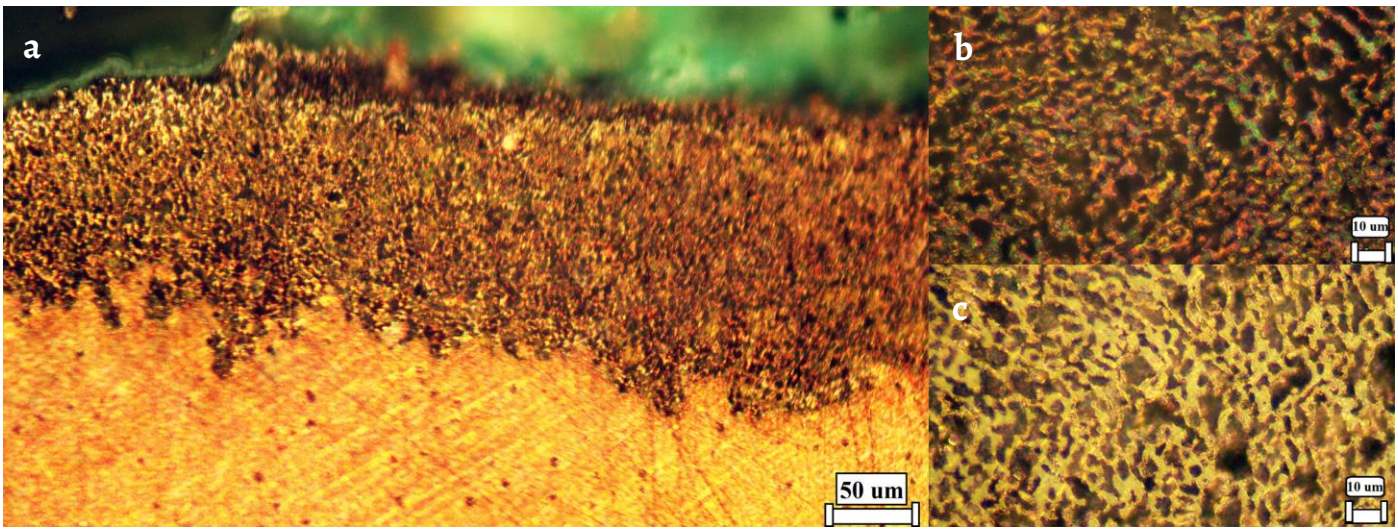

Figure 4. PLM images for the cross–section of the snake–shaped bracelet demonstrating: *a)* unetched corrosion and alloy layers. And the details of the etched: *b)* silver rich alloy zone, and *c)* copper rich alloy zone.

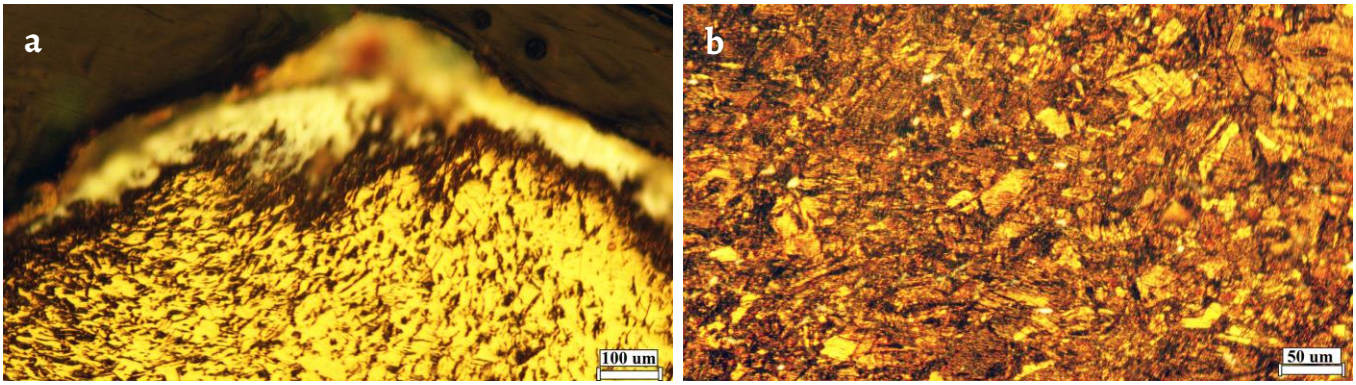

Figure 5. PLM images of the flat–spoon spatula: *a)* the unetched corroded edge; *b)* etched internal alloy.

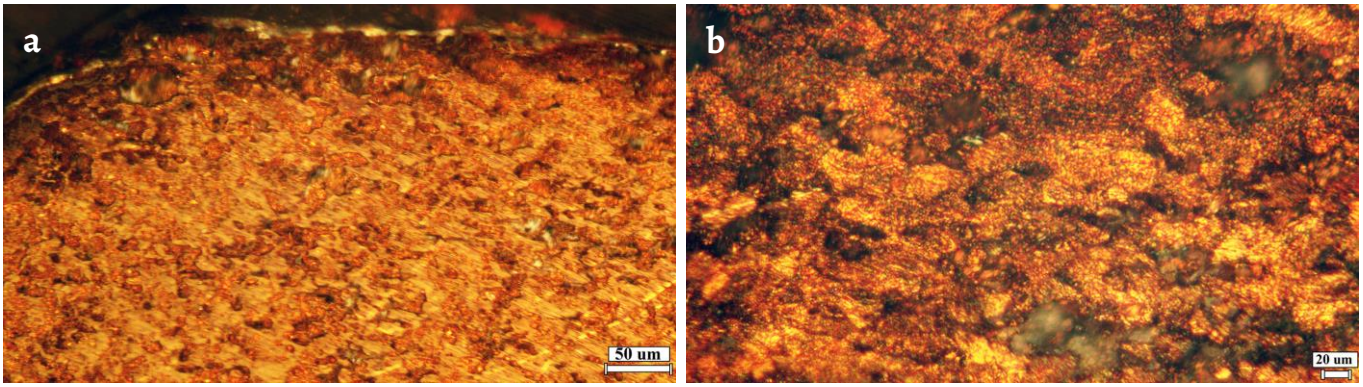

Figure 6. PLM images of the twisted–handle spatula: *a)* the unetched corroded edge; *b)* the etched internal alloy.

For the flat–spoon spatula, the examination of its unetched cross–section using the PLM shows a large amount of lead near the edge of the cross–section. In leaded copper alloys, the lead usually occurs as spherical globules dispersed at the grain boundaries of the alloy, however with high lead content, some gravity segregation may take the lead down to the base or bottom of the mold in the casting process [32, 47]. Therefore, the lead is not uniformly distributed, and a high amount is located near the external surface of the spatula (Figure 5a). Upon cooling after the casting, the lead was separated from the alloy towards the external surface. The lead concentrated near the surface would have given this spatula a grayer shade to the golden color of copper–zinc brass. The partially recrystallized grains of the etched internal alloy indicate that the cast artifact was annealed for a short period of time at high temperature or for a longer period at moderate temperatures. The presence of slightly curved annealing twins and a series of slip lines implies some cold working without sufficient annealing to give the artifact its final shape (Figure 5b) [32, 53–54]. It should be noted that not all alloys are suitable for being hot–worked, leaded brass alloys such as the alloy of this spatula are considered a "hot–short", which implies that they will tend to break apart on hot–working or become brittle [47].

For the twisted–handle spatula, the top side of the unetched cross–section's PLM image shows a corroded tin–rich α+δ eutectoid underneath the red cuprite layer (Figure 6a). Investigating the internal alloy microstructure after etching at higher magnification shows a cored distorted dendritic microstructure (Figure 6b), which suggests that the cast object was cold–worked without annealing. The micrograph also shows some porosity that was not eliminated by cold working and some unrefined copper sulfide ore inclusions [32, 36].

Microhardness testing

The microhardness testing results show that the average hardness value is about 114.7 ± 0.9 HV for the twisted–strands bracelet, which is consistent with a quaternary copper–zinc–tin–lead alloy that was worked and annealed in the manufacturing process. On the other hand, the snake–shaped bracelet has two hardness values: 97.5 ± 1.3 HV for the internal copper rich alloy

zone and 25.7 ± 0.6 HV for the external silver rich alloy zone, which is attributed to the higher hardness of copper in comparison with that of silver and the presence of zinc as a third alloying element. The flat–spoon spatula has a 125.4 ± 9.6 HV microhardness value, which matches the expected value for a leaded brass alloy that was cold worked without sufficient annealing to give the object its final shape. The highest microhardness value was 168.7 ± 7.5 HV for the twisted–handle spatula, which conforms with a 9 % tin bronze alloy that was cold–worked without annealing after the casting process of the object. The microhardness testing results are in accordance with the SEM/EDX alloy elemental analysis and metallographic examination results. The variation in the microhardness values of the artifacts is attributed to their compositional differences and various degrees of working and heat treatment [32, 47].

Cathodic polarization scans

The cathodic polarization scans of the artifacts plotted as (Log (current) vs potential) are shown in Figure 7. The twisted–strands bracelet was scanned from E_{corr} at (−0.48 V) to (−1.80 V) in 1 % sodium sesquicarbonate, its cathodic polarization curve in Figure 7 shows three reduction shoulder peaks; the first starts after −0.55 V and can be attributed to the reduction of the basic cupric chloride ($Cu_2(OH)_3Cl$) corrosion products. The second starts at about −0.87 V and reaches its maximum at about −1.00 V and could be attributed to the reduction of cuprous oxide (Cu_2O), this is followed by the third small peak that ends at about −1.34 V and could be attributed to the reduction of the basic cupric carbonate ($CuCO_3.Cu(OH)_2$) corrosion product. The hydrogen evolution potential starts after −1.40 V [23, 29, 55].

The snake–shaped bracelet was scanned from E_{corr} (−0.40 V) to (−1.80 V). Its cathodic polarization curve in Figure 7 shows a reduction peak that starts at about −0.55 V and could be attributed to the reduction of the chloride-based corrosion products of silver and copper (AgCl, $Cu_2(OH)_3Cl$) [56–57]. The plateau around −1.00 V and the shoulder at about −1.30 V could be attributed to the reduction of Cu_2O and $CuCO_3.Cu(OH)_2$ respectively. The progressive increase in the current density after −1.40 V is assigned to the hydrogen evolution reaction.

For the flat–spoon spatula, the potential was scanned cathodically from the E_{corr} at (−0.48 V) to (−1.80 V). The cathodic polarization curve obtained in Figure 7 shows a small reduction peak that starts at about −0.59 V, which could be referred to the reduction of $Cu_2(OH)_3Cl$. This is followed by a long reduction plateau between −0.79 V and −1.05 V, which could be attributed to the reduction of Cu_2O and probably CuO. The reduction slope around −1.30 V is attributed to the reduction of $CuCO_3.Cu(OH)_2$, it is followed by the hydrogen evolution potential after −1.40 V as previously mentioned.

Similarly, the potential for the twisted–handle spatula was scanned cathodically from the E_{corr} (−0.47 V) to (−1.80 V). The cathodic polarization curve obtained in Figure 7 shows a reduction hump that starts after −0.60 V and can be attributed to chloride–based corrosion products ($Cu_2(OH)_3Cl$). The second reduction peak starts at about −0.85 V and reaches its maximum at about −1.00 V, which could be attributed to the reduction of Cu_2O. The third reduction slop starts at about −1.12 V and could be attributed to the reduction of $CuCO_3.Cu(OH)_2$. As for the other artifacts, the hydrogen evolution potential starts after −1.40 V [23, 29, 55].

It should be noted that the analysis of the cathodic polarization curves concentrated on the major corrosion products of the main metals in the alloys, therefore the reduction potentials of possible minor corrosion products of the small alloying elements in the bronze or quaternary alloy artifacts were excluded.

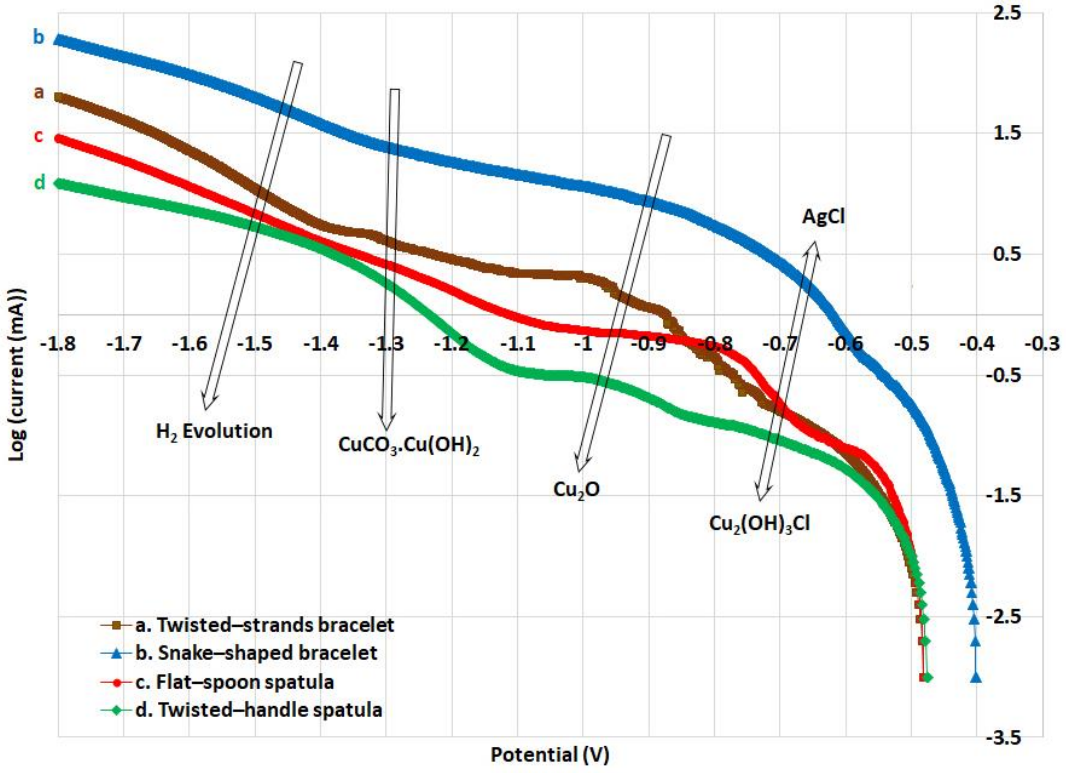

Figure 7. Cathodic polarization scans of the artifacts in 1 % w/v ($Na_3H(CO_3)_2{\cdot}2H_2O$) solution.

Potentiostatic reduction

Based on the cathodic polarization scan results and comparable literature data, a constant potential of –1.4 V is sufficient to reduce the corrosion products appearing on the copper alloy artifacts and avoid vigorous hydrogen evolution on the surface during the treatment. The process continued until the current reached a low stable value, which indicated the completion of the reduction process. As Figure 8 shows, monitoring the current of twisted–strands bracelet showed that it started from about 29.1 mA at the beginning of the potentiostatic reduction process and decreased to a stable low value of about 2.6 mA after 30 h. Similarly, for the snake–shaped bracelet, the reduction current decreased from 75 mA to 6.3 mA in about 30 h of the potentiostatic reduction process. In the case of the flat–spoon spatula, the reduction current decreased from about 21.8 mA to a low stable value of about 2.1 mA indicating the completion of the reduction process after 22 h. Finally, for the twisted–handle spatula, the current started at 21.3 mA and reached about 6.8 mA after 28 h of the potentiostatic reduction at –1.4 V. The beauty of using such low current densities at a steady voltage is that there is a much greater chance of retention of the original profiles of the artifacts.

The potentiostatic reduction treatment converted the corrosion products on the artifacts to a reduced metal deposited with weak cohesion to the surface. After the completion of the reduction process, the artifacts had mottled dark layers, therefore they were rinsed under running water with gentle brushing from a camel hair artist's brush to clean the reduction residues and improve their appearance, and the copper spots on the surface of the snake–shaped bracelet were wiped with cotton swabs moistened with a diluted solution of silver nitrate ($AgNO_3$) to unify its silvery appearance [30].

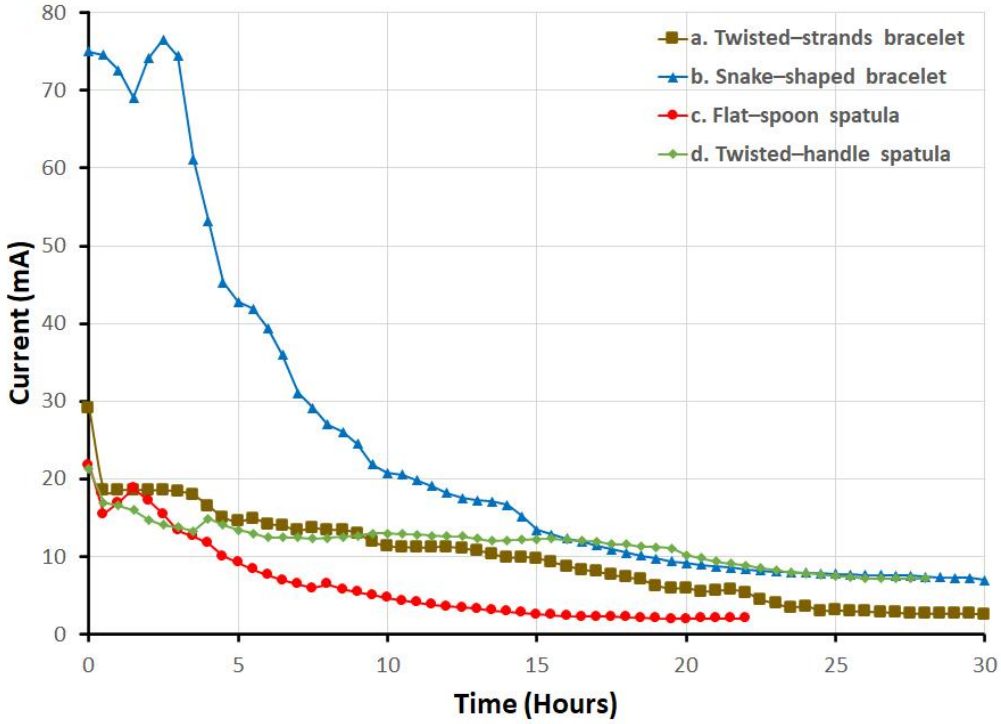

Figure 8. Chronoamperometric curves for the potentiostatic reduction of corrosion products on the artifacts in 1 % w/v ($Na_3H(CO_3)_2{\cdot}2H_2O$) solution.

Finally, the artifacts were cleaned with deionized water then dried in acetone. Since they were going back to their environmentally uncontrolled storage area, they were coated with a 3 % Paraloid B72 solution to protect them against environmental agents of deterioration that may cause corrosion such as high relative humidity and pollutant gases. Paraloid B72 is an ethyl methacrylate and methyl acrylate co-polymer with a molar ratio of 70:30 %. It is widely used by metal conservators to coat metals artifacts due to its good adhesion, relative long term stability, transparency, mechanical resistance and reversibility [12, 58–59]. The 3 % Paraloid B72 solution was applied by brushing for three times to form a protective coating layer on the artifacts, and the edge of the flat–spoon spatula was fixed to its handle using a 20 % Paraloid B72 adhesive. The repeated coating is needed to ensure that there is sufficient dry film thickness over the convoluted and microporous surface. Figure 9 shows the images of the artifacts after the end of the treatment.

Figure 9. After the treatment: *a)* twisted–strands bracelet; *b)* snake–shaped bracelet; *c)* flat–spoon spatula; *d)* twisted–handle spatula.

Conclusion

The spectroscopic and microscopic analytical investigation of the copper alloy artifacts from the archaeological cemetery that was located on the site of the Queen Ali International Airport site presented the required information to understand their composition, microstructural characteristics, and state of preservation. The cathodic polarization curves of the artifacts in the sodium sesquicarbonate solution were effective in identifying the required working parameters to reduce their corrosion products while avoiding over potential causing vigorous

hydrogen evolution. The monitoring of the corrosion potentiostatic reduction process by chronoamperometry was effective in determining the end of the process. The use of the potentiostatic reduction method helped to preserve the original surface details of the artifacts and prevent aggressive treatment. The versatility and effectiveness of controllable electrochemical methods provide a safe and effective conservation alternative to stabilize actively corroded artifacts, which can then be coated with a conservation grade coating or maintained in an environmentally controlled exhibition or storage area.

Acknowledgements
I would like to thank the Deanship of Scientific Research and Graduate Studies at Yarmouk University for funding this research. I would also like to thank Professor Moawiya Ibrahim for kindly offering me written permission to work on the artifacts and publish the results. Thanks are also extended to Dr. Ian MacLeod for the very constructive and useful comments on the draft of the paper.

REFERENCES

1. Ingo, G. M.; Riccucci, C.; Guida, G.; Albini, M.; Giuliani, C.; Di Carlo, G., 'Rebuilding of the burial environment from the chemical biography of archaeological copper-based artifacts', *ACS Omega* **4** (2019) 11103–11111, https://doi.org/10.1021/acsomega.9b00569.
2. Abu-Baker, A. N.; Khalil, L.A., 'An analytical study of the corrosion behavior and microstructural properties of a group of copper alloy artifacts from the Khirbet Yajuz archaeological site, Jordan', in *Metal2022: Proceedings of the Interim Meeting of the ICOM-CC Metals Working Group*, eds. P. Mardikian, L. Näsänen, and A. Arponen, International Council of Museums – Committee for Conservation (ICOM–CC) and The National Museum of Finland, Helsinki (2022) 221–230.
3. Oudbashi, O.; Bahadori, S.; Aliyari, A., 'Corrosion Analysis and Assessment of a Collection of Archaeological Copper Alloy Objects from Sagzabad, Northern Iran', in *Metal2022: Proceedings of the Interim Meeting of the ICOM-CC Metals Working Group*, eds. P. Mardikian, L. Näsänen, and A. Arponen, International Council of Museums – Committee for Conservation (ICOM–CC) and The National Museum of Finland, Helsinki (2022) 231–239.
4. Thunberg, J. C.; Emmerson, N. J.; Harsányi, I.; Lewis, M.; Watkinson, D. E.; Kis, Z.; Kasztovszky, Z., 'The Role of Patina on Archaeological Copper Alloy Coins in the Outbreak and Progression of Bronze Disease', in *Metal2022: Proceedings of the Interim Meeting of the ICOM-CC Metals Working Group*, eds. P. Mardikian, L. Näsänen, and A. Arponen, International Council of Museums – Committee for Conservation (ICOM–CC) and The National Museum of Finland, Helsinki (2022) 203–211.
5. Plenderleith, H. J., The conservation of antiquities and works of art: treatment, repair and restoration, Oxford University Press, London (1957) 232–257.
6. Organ, R. M., 'The examination and treatment of bronze antiquities', *Studies in Conservation* **6**(sup1) (1961) 104–110, https://doi.org/10.1179/sic.1961.s026.
7. Hamilton, D. L., *Methods of conserving underwater archaeological material culture*, Conservation files: ANTH 605, Conservation of Cultural Resources I. Nautical Archaeology Program, Texas A&M University, (1999), https://files.pca-cpa.org/pcadocs/ua-ru/04.%20UA%20Rejoinder%20Memorial/01.%20Exhibits/UA-116.pdf (accessed 2021-09-19).
8. MacLeod, I. D., 'Conservation of corroded copper alloys: a comparison of new and traditional methods for removing chloride ions', *Studies in Conservation* **32**(1) (1987) 25–40, https://doi.org/10.1179/sic.1987.32.1.25.
9. North, N. A., *Conservation of metals, in Conservation of marine archaeological objects*, ed. C. Pearson, Butterworths, London (1987), 207–252, https://doi.org/10.1016/B978-0-408-10668-9.50016-2.
10. Pearson, C., 'On-site storage and conservation', in *Conservation of marine archaeological objects*, ed. C. Pearson, Butterworths, London (1987) 105–116, https://doi.org/10.1016/B978-0-408-10668-9.50012-5.
11. Faltermeier, R. B., 'A corrosion inhibitor test for copper-based artifacts', *Studies in Conservation* **44**(2) (1999) 121–128, https://doi.org/10.1179/sic.1999.44.2.121.
12. Argyropoulos, V.; Giannoulaki, M.; Michalakakos, G. P.; Siatou, A., 'A survey of the types of corrosion inhibitors and protective coatings used for the conservation of metal objects from museum collections in the Mediterranean basin', in *Strategies for saving our cultural heritage*, eds. V. Argyropoulos, A. Hein, and M.A. Harith, TEI of Athens, Athens (2007) 1–5.
13. Mezzi, A.; Angelini, E.; De Caro; T.; Grassini, S.; Faraldi, F.; Riccucci, C.; Ingo, G. M., 'Investigation of the benzotriazole inhibition mechanism of bronze disease', *Surface and Interface Analysis* **44**(8) (2012) 968–71, https://doi.org/10.1002/sia.4841.
14. Abu-Baker, A. N.; MacLeod, I. D.; Sloggett, R.; Taylor, R., 'A comparative study of salicylaldoxime, cysteine and benzotriazole as inhibitors for the active chloride-based corrosion of copper and bronze artifacts', *European Scientific Journal* **9**(33) (2013) 228–251, https://doi.org/10.19044/esj.2013.v9n33p%25p.
15. Cano, E.; Lafuente, D., 'Corrosion inhibitors for the preservation of metallic heritage artefacts', in *Corrosion and conservation of cultural heritage metallic artefacts*, eds. P. Dillmann, D. Watkinson, E. Angelini, and A. Adriaens, Woodhead Publishing, Cambridge (2013) 570–594, https://doi.org/10.1533/9781782421573.5.570.

16. Hassairi, H.; Bousselmi, L.; Khosrof, S.; Triki, E., 'Evaluation of the inhibitive effect of benzotriazole on archeological bronze in acidic medium', *Applied Physics A* **113**(4) (2013) 923–931, https://doi.org/10.1007/s00339-013-7719-y.
17. Abu-Baker, A. N.; Al-Qudah, M. A., 'A new dioxime corrosion inhibitor for the protection and conservation of copper: synthesis, characterization and evaluation in acidic chloride solution', *Applied Physics A* **122**(8) (2016) 765, https://doi.org/10.1007/s00339-016-0289-z.
18. Abu-Baker, A. N.; Al-Qudah, M.A., 'A novel dioxime compound for protecting copper in neutral chloride solutions and to treat bronze disease in archaeological artefacts', *AICCM Bulletin* **38**(2) (2017) 94–102, https://doi.org/10.1080/10344233.2017.1407865.
19. Abu-Baker, A. N., 'From mono-oxime to tri-oxime: the development of a new group of corrosion inhibitors for copper alloys', in *Metal2019: Proceedings of the Interim Meeting of the ICOM-CC Metals Working Group*, eds. C. Chemello, L. Brambilla, and E. Joseph, International Council of Museums–Committee for Conservation (ICOM-CC) and Haute Ecole Arc Conservation-Restauration (HE-Arc CR), Neuchâtel (2019) 204–211.
20. Abu-Baker, A. N.; Khalil, L. A.; Al-Gonmeen, T., 'A multi-analytical exploration of the chemical composition, microstructural properties and corrosion inhibiting treatment for an archaeological brass censer from Umm Zuwaytinah, Amman', *Nuclear Instruments and Methods in Physics Research Section B* **502** (2021) 73–79, https://doi.org/10.1016/j.nimb.2021.06.008.
21. Joseph, E., 'Biopassivation method for the preservation of copper and bronze artefacts', *Frontiers in Materials* **7** (2021) 475, https://doi.org/10.3389/fmats.2020.613169.
22. Païn, S.; Bertholon, R.; Lacoudre, N., 'La dechloruration des alliages cuivreux par electrolyse a faible polarisation dans le sesquicarbonate de sodium', *Studies in Conservation* **36**(1) (1991) 33–43, https://doi.org/10.2307/1506450.
23. Bertholon, R.; Bell, B.; Blengino, J. M.; Lacoudre, N., 'Stabilisation de la corrosion d'un objet archéologique en alliage cuivreux par électrolyse à faible polarisation dans le sesquicarbonate de sodium: dernières experiences', in *Metal 95: Proceedings of the International Conference on Metals Conservation*, eds. I. D. MacLeod, S. L. Pennec, and L. Robbiola, James & James, London (1997) 209–219.
24. Costa, V., 'Electrochemistry as a conservation tool: an overview', in *Conservation Science 2002*, eds. J. Townsend, K. Eremin, and A. Adriaens, Archetype Publications, London (2003) 88– 95.
25. Ehanti, E., 'Optimization of electrolytic stabilization of marine archaeological copper alloys', *BROMEC* **14** (2005) 11, https://warwick.ac.uk/fac/sci/physics/research/condensedmatt/sims/bromec/bromec_14_english.pdf (accessed 2021-09-19).
26. Adriaens, A.; Dowsett, M.; Leyssens, K.; Van Gasse, B., 'Insights into electrolytic stabilization with weak polarization as treatment for archaeological copper objects', *Analytical and Bioanalytical Chemistry* **387** (3) (2007) 861–868, https://doi.org/10.1007/s00216-006-0835-1.
27. Costa, V., 'The deterioration of silver alloys and some aspects of their conservation', *Studies in Conservation* **46**(sup1) (2001) 18–34, https://doi.org/10.1179/sic.2001.46.Supplement-1.18.
28. Degrigny, C.; Jeanneret, R.; Witschard, D., 'Local cleaning with the pleco electrolytic pencil of the tarnished saint candide reliquary head at the treasury of Saint-Maurice Abbey, Valais (Switzerland)', *e-Preservation Science* **12** (2015) 20–27.
29. Selwyn, L.; McKinnon, W. R., 'Practical electrochemistry for conservators and conservation scientists: part II: characterizing and treating corroded metals', *Journal of the Canadian Association for Conservation* **42** (2017) 16–32.
30. Abu-Baker, A. N.; MacLeod, I. D., 'An electrochemical simulation and treatment study for the carbonate and chloride based corrosion of heritage silver–copper alloys', *Studies in Conservation* **66**(4) (2021) 190–210, https://doi.org/10.1080/00393630.2020.1796020.
31. Ibrahim, M. M.; Gordon, R. L., *A cemetery at Queen Alia International Airport*, Yarmouk University, Irbid (1987).
32. Scott, D. A., *Metallography and microstructure of ancient and historic metals*, The Getty Conservation Institute, Los Angeles (1992).
33. Eary, L. E., 'Geochemical and equilibrium trends in mine pit lakes', *Applied Geochemistry* **14**(8) (1999) 963–987, https://doi.org/10.1016/S0883-2927(99)00049-9.
34. MacLeod, I. D., 'Bronze disease: an electrochemical explanation', *ICCM Bulletin* **7**(1) (1981) 16–26, https://doi.org/10.1179/iccm.1981.7.1.002.
35. Scott, D. A., 'Bronze disease: a review of some chemical problems and the role of relative humidity', *Journal of the American Institute for Conservation* **29**(2) (1990) 193–206, https://doi.org/10.1179/019713690806046064.
36. Abu-Baker, A., 'Investigating the corrosion and microstructure of five copper-based archaeological artefacts from Tell el-Ajjul', *AICCM Bulletin* **31**(1) (2008) 87–96, https://doi.org/10.1179/bac.2008.31.1.008.
37. Fierascu, R. C.; Ion, R. M.; Fierascu, I., 'Archaeometallurgical characterization of numismatic artifacts', *Instrumentation Science and Technology* **43**(1) (2015) 107–114, https://doi.org/10.1080/10739149.2014.961642.
38. Craddock, P. T., 'The composition of the copper alloys used by the Greek, Etruscan and Roman civilizations: 3. The origins and early use of brass', *Journal of Archaeological Science* **5**(1) (1978) 1–16, https://doi.org/10.1016/0305-4403(78)90015-8.
39. Čechák, T.; Hložek, M.; Musílek, L.; Trojek, T., 'X-ray fluorescence in investigations of archaeological finds', *Nuclear Instruments and Methods in Physics Research Section B* **263**(1) (2007) 54–57, https://doi.org/10.1016/j.nimb.2007.04.176.
40. Hörz, G.; Kallfass, M., 'The treasure of gold and silver artifacts from the Royal Tombs of Sipán, Peru –a study on the Moche metalworking techniques', *Materials Characterization* **45**(4–5) (2000) 391–419, https://doi.org/10.1016/S1044-5803(00)00093-0.
41. Giumlia-Mair, A., 'Plating and surface treatments on ancient metalwork', *Advances in Archaeomaterials* **1**(1) (2020) 1–26, https://doi.org/10.1016/j.aia.2020.10.001.
42. Angelini, E.; de Caro, T.; Mezzi, A.; Riccucci, C.; Faraldi, F.; Grassini, S., 'Degradation Mechanisms Occurring in Precious Metallic Artefacts', *Surface and Interface Analysis* **44**(8) (2012) 947–952, https://doi.org/10.1002/sia.3854.
43. Mezzi, A.; De Caro, T.; Riccucci, C.; Angelini, E.; F. Faraldi, F.; Grassini, S., 'Micro-chemical Surface Investigation of Brittle Carthaginian and Roman Silver Artefacts', *Surface and Interface Analysis* **44**(8) (2012) 972–976, https://doi.org/10.1002/sia.4845.

44. Thornton, C. P., 'Of brass and bronze in prehistoric Southwest Asia', in *Metals and mines: studies in archaeometallurgy*, eds. S. La Niece, D. Hook, and P. Craddock, Archetype Publications and British Museum, London (2007) 123–135.
45. Bottaini, C.; Mirão, J.; Candeias, A.; Catarino, H.; Silva, R. J.; Brunetti, A., 'Elemental characterisation of a collection of metallic oil lamps from South-Western al-Andalus using EDXRF and Monte Carlo simulation', *European Physical Journal Plus* **134** (2019) 365, https://doi.org/10.1140/epjp/i2019-12894-4.
46. El-Mahdy, G. A., 'Electrochemical impedance study on brass corrosion in NaCl and $(NH_4)_2SO_4$ solutions during cyclic wet–dry conditions', *Journal of Applied Electrochemistry* **35**(3) (2005) 347–353, https://doi.org/10.1007/s10800-004-8347-1.
47. Scott, D. A.; Schwab, R., *Metallography in art and archaeology (cultural heritage science)*, Springer Nature, Switzerland (2019), https://doi.org/10.1007/978-3-030-11265-3.
48. MacLeod, I.; Wozniak, R., 'Corrosion and conservation of tin and pewter', in *Metal 95: Proceedings of the ICOM-CC Metals Working Group Conference*, eds. I. MacLeod, S. Pennec, and L. Robbiola, James & James, London (1997) 118–123.
49. Strandberg, H.; Johansson, L.; Lindqvist, O., 'The atmospheric corrosion of statue bronzes exposed to SO_2 and NO_2', *Materials and Corrosion* **48** (1997) 721–730, https://doi.org/10.1002/maco.19970481102.
50. Ingo, G. M.; Çilingiroğlu, A.; Faraldi, F.; Riccucci, C.; Casaletto, M. P.; Erdem, A.; Batmaz, A., 'The bronze shields found at the Ayanis fortress (Van region, Turkey): manufacturing techniques and corrosion phenomena', *Applied Physics A* **100** (2010) 793–800, https://doi.org/10.1007/s00339-010-5656-6.
51. Żmuda-Trzebiatowska, I.; del Hoyo-Meléndez, J. M.; Śliwiński, G., 'Material composition evaluation of historical Cu alloy aquamanilia by complementary XRF and LIBS measurements', *European Physical Journal Plus* **134** (2019) 269, https://doi.org/10.1140/epjp/i2019-12705-0.
52. Scott, D. A., *Ancient metals: microstructure and metallurgy volume I*, Conservation Science Press, Los Angeles (2012).
53. Giannossa, L. C.; Loperfido, S.; Caggese, M.; De Benedetto, G. E.; Laviano, R.; Sabbatini, L.; Mangone, A., 'A systematic characterization of fibulae from Italy: from chemical composition to microstructure and corrosion processes', *New Journal of Chemistry* **37**(4) (2013) 1238–1251, https://doi.org/10.1039/C2NJ40362E.
54. Delrue, P., *Archaeometallurgical analyses of pre-Islamic artefacts from ed-Dur (Emirate of Umm al-Qaiwain, U.A.E.*, PhD dissertation, University of Ghent (2008), https://biblio.ugent.be/publication/4147771/file/4147778.pdf, (accessed 2021-09-19).
55. Leyssens, K.; Adriaens, A.; Degrigny, C., 'Electrochemical monitoring of the storage or stabilization of archaeological copper based artefacts in sodium sesquicarbonate solutions', in *ICOM-CC 14th Triennial Meeting preprint*, ed. I. Sourbès-Verger, James & James, London (2005) 301–309.
56. Zaky, A. M., 'Electrochemical behaviour of copper–silver alloys in sodium carbonate aqueous solution', *British Corrosion Journal* **36**(1) (2001) 59–64, https://doi.org/10.1179/ 000705901101501505.
57. Zaky, A. M., 'Role of Cl^- in breakdown of Cu–Ag alloys passivity in aqueous carbonate solutions', *Electrochimica Acta* **51**(10) (2006) 2057–2062, https://doi.org/10.1016/j.electacta.2005.07.013.
58. Carmen, L. I., 'Biodeterioration of acrylic polymers Paraloid B-72 and B-44: Report on field trials', *Anatolian Archaeological Studies* **15**(2016) 283–289.
59. Vinçotte, A.; Beauvoit, E.; Boyard, N.; Guilminot, E., 'Effect of solvent on PARALOID® B72 and B44 acrylic resins used as adhesives in conservation', *Heritage Science* **7** (2019) 42, https://doi.org/10.1186/s40494-019-0283-9.

RECEIVED: 2022.1.20
REVISED: 2022.5.10
ACCEPTED: 2022.10.16
ONLINE: 2023.4.5